

Integrated exploration of turbulent cross-helicity effect: theory, observation, modeling and numerical simulations of the solar convection zone

By N. Yokoi[†], G. Balarac[‡], I. N. Kitiashvili, N. Kleeorin[¶],
A. G. Kosovichev^{||}, I. Rogachevskii^{||} AND R. Simitev^{††}

Cross helicity (velocity–magnetic-field correlation) is one of the basic quantities in magnetohydrodynamics. In the presence of large-scale vortical motion, if there is positive (or negative) cross helicity in turbulence, a contribution to the electromotive force parallel (or anti-parallel) to the large-scale vorticity arises. By considering the evolution equation of turbulent cross helicity, the mechanisms that create turbulence with cross helicity are investigated. In order to analyze cross helicity-related transport and cross-helicity generation mechanisms, three kinds of numerical simulations are performed: (i) direct numerical simulations of the local Kolmogorov flow with an imposed magnetic field, (ii) global direct simulation of a rotating spherical fluid shell, and (iii) large-eddy simulation of the local compressible flow near the sunspot region. Through these simulations, the importance of the cross-helicity effect is validated. The cross-helicity generation mechanisms relevant to the incompressible and compressible cases are also discussed.

1. Introduction

Because of the coupling between the velocity and magnetic fields, magnetohydrodynamic (MHD) turbulence shows very interesting nonlinear behavior. Magnetic fields are induced by turbulent fluid motion, and the generated fields influence the turbulence. These are strong effects in MHD flows. At large magnetic Reynolds number [$Rm(= uL/\eta)$, u : characteristic velocity, L : characteristic length, η : magnetic diffusivity], the induced magnetic field is sometimes much larger in magnitude than the original or imposed field. If the tendency of the magnetic field to be advected by fluid motion is very strong, the magnetic field can be considered as frozen into the plasma motion. In such a high Rm flow, the turbulent cross helicity, the velocity–magnetic-field correlation of turbulence, is a quantity of primary importance. The most important property of the cross helicity is related to the turbulent dynamo. The mean magnetic field obeys the mean induction equation:

$$\frac{\partial \mathbf{B}}{\partial t} = \nabla \times (\mathbf{U} \times \mathbf{B}) + \nabla \times \mathbf{E}_M + \eta \nabla^2 \mathbf{B}. \quad (1.1)$$

Here \mathbf{E}_M is the turbulent electromotive force defined by

$$\mathbf{E}_M \equiv \langle \mathbf{u}' \times \mathbf{b}' \rangle. \quad (1.2)$$

[†] Institute of Industrial Science, University of Tokyo

[‡] Laboratoire des Écoulements Géophysiques et Industriels, University of Grenoble

[¶] Department of Mechanical Engineering, Ben-Gurion University of Negev

^{||} Hansen Experimental Physics Laboratory, Stanford University

^{††} Department of Mathematics, University of Glasgow

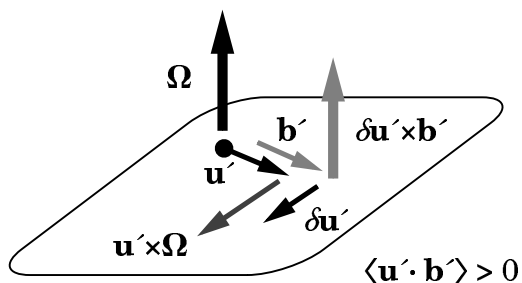


FIGURE 1. Physical interpretation of the cross-helicity effect.

This quantity is of primary importance in MHD turbulence theory since it contains the effect of turbulence in the mean magnetic induction equation (1.1).

In the presence of large-scale vorticity $\mathbf{\Omega} (= \nabla \times \mathbf{U})$, cross helicity in the turbulence may lead to a turbulent electromotive force aligned with the large-scale vorticity (figure 1). We consider a fluctuating fluid element with large-scale vorticity and assume there is a positive correlation between the velocity and magnetic fields in the turbulence ($\langle \mathbf{u}' \cdot \mathbf{b}' \rangle > 0$). The fluid element is subject to a Coriolis-like force due to local angular-momentum conservation, and the induced velocity is $\delta \mathbf{u}' [= \tau(\mathbf{u}' \times \mathbf{\Omega})]$ (τ : time scale). By assumption, the magnetic fluctuation \mathbf{b}' is statistically aligned with the velocity fluctuation \mathbf{b}' . As a consequence, the contribution to the electromotive force is written as

$$\langle \delta \mathbf{u}' \times \mathbf{b}' \rangle = \tau \langle \mathbf{u}' \cdot \mathbf{b}' \rangle \mathbf{\Omega}. \quad (1.3)$$

Thus, this assumption has the result that the combination of large-scale vortical motion and positive (or negative) turbulent cross helicity gives rise to an electromotive force parallel (or anti-parallel) to the mean vorticity.

With this effect in mind, it is quite natural that the turbulent electromotive force is expressed as

$$\mathbf{E}_M = \alpha \mathbf{B} - \beta \mathbf{J} + \gamma \mathbf{\Omega}. \quad (1.4)$$

Here we should note that electromotive force \mathbf{E}_M and the electric current density $\mathbf{J} (= \nabla \times \mathbf{B})$ are polar vectors whereas the magnetic field \mathbf{B} and the vorticity $\mathbf{\Omega}$ are axial vectors. As a result, the coefficients α and γ are pseudo-scalar whereas β is a pure scalar.

It is known that the coefficients α , β , and γ can be expressed in terms of the turbulent residual helicity $H \equiv \langle \mathbf{b}' \cdot \mathbf{j}' - \mathbf{u}' \cdot \boldsymbol{\omega}' \rangle$, the turbulent MHD energy $K \equiv \langle \mathbf{u}'^2 + \mathbf{b}'^2 \rangle / 2$, and the turbulent cross helicity $W \equiv \langle \mathbf{u}' \cdot \mathbf{b}' \rangle$, respectively (Pouquet *et al.* 1976; Krause & Rädler 1980; Yoshizawa 1990). They are modeled as

$$\alpha = C_\alpha \tau \langle \mathbf{b}' \cdot \mathbf{j}' - \mathbf{u}' \cdot \boldsymbol{\omega}' \rangle = C_\alpha \tau H, \quad (1.5a)$$

$$\beta = C_\beta \tau \langle \mathbf{u}'^2 + \mathbf{b}'^2 \rangle / 2 = C_\beta \tau K, \quad (1.5b)$$

$$\gamma = C_\gamma \tau \langle \mathbf{u}' \cdot \mathbf{b}' \rangle = C_\gamma \tau W, \quad (1.5c)$$

with C_α , C_β , and C_γ being the model constants. Here τ is the characteristic time of turbulence, which is often expressed as

$$\tau = K / \varepsilon, \quad (1.6)$$

with the dissipation rate of the turbulent MHD energy, ε , defined by

$$\varepsilon = \nu \left\langle \frac{\partial u'^a}{\partial x^b} \frac{\partial u'^a}{\partial x^b} \right\rangle + \eta \left\langle \frac{\partial b'^a}{\partial x^b} \frac{\partial b'^a}{\partial x^b} \right\rangle. \quad (1.7)$$

Substituting (1.4) into (1.1), we have

$$\frac{\partial \mathbf{B}}{\partial t} = \nabla \times (\mathbf{U} \times \mathbf{B}) + \nabla \times (\alpha \mathbf{B} + \gamma \boldsymbol{\Omega}) - \nabla \times [(\eta + \beta) \nabla \times \mathbf{B}]. \quad (1.8)$$

This shows that the β -related term in (1.4) represents the enhancement of the magnetic diffusivity due to turbulence ($\eta \rightarrow \eta + \beta$), which is called the turbulent magnetic diffusivity or turbulent resistivity. On the other hand, the α - and γ -related terms represent possible magnetic-field generation mechanisms due to pseudo-scalars in turbulence. They are called the α or helicity effect and the cross-helicity effect, respectively.

In the history of turbulent dynamo research, the cross-helicity effect has been neglected. This is in strong contrast to the α or helicity effect, which has been studied extensively. However, as we have just seen, the presence of turbulent cross helicity in the large-scale vortical field leads to the cross-helicity effect. Large-scale rotational motion is ubiquitous in astro- and geophysical phenomena. Thus, it is highly desirable to examine the validity of the cross-helicity dynamo in the astro- and geophysical contexts. The most important problem is to see how and how much cross helicity can exist in turbulence in the presence large-scale inhomogeneities such as velocity shear, rotation, density stratification, etc. This problem is addressed in this work with the aid of three kinds of numerical simulations. Through these simulations, we examine how the cross helicity is spatially distributed, how it is generated, how strong it is, etc.

The organization of this paper is as follows. In section 2, the evolution equation of the cross helicity is presented with special emphasis on the generation mechanisms of the turbulent cross helicity. In section 3, some results of three numerical simulations are presented. In section 4, the cross-helicity generation mechanisms and the magnitude of the turbulent cross helicity scaled by the turbulent MHD energy are discussed in comparison with the theoretical prediction on the magnitude of the torsional oscillation. Concluding remarks are given in section 5.

2. Cross-helicity equation

The turbulent cross helicity (density) $\langle \mathbf{u}' \cdot \mathbf{b}' \rangle$ obeys a simple evolution equation. In an incompressible MHD case, it is written as

$$\left(\frac{\partial}{\partial t} + \mathbf{U} \cdot \nabla \right) W = P_W - \varepsilon_W + T_W, \quad (2.1)$$

where P_W , ε_W , and T_W are the production, dissipation, and transport rates of the turbulent cross helicity, respectively. They are defined by

$$P_W = -\mathcal{R}^{ab} \frac{\partial B^a}{\partial x^b} - \mathbf{E}_M \cdot \boldsymbol{\Omega}, \quad (2.2a)$$

$$\varepsilon_W = (\nu + \eta) \left\langle \frac{\partial u'^a}{\partial x^b} \frac{\partial b'^a}{\partial x^b} \right\rangle, \quad (2.2b)$$

$$T_W = \mathbf{B} \cdot \nabla K + \nabla \cdot \left\langle -(\mathbf{u}' \cdot \mathbf{b}') \mathbf{u}' + \left(\frac{\mathbf{u}'^2 + \mathbf{b}'^2}{2} - p'_M \right) \mathbf{b}' \right\rangle, \quad (2.2c)$$

where \mathcal{R} is the Reynolds stress defined by

$$\mathcal{R}^{\alpha\beta} = \langle u'^{\alpha} u'^{\beta} - b'^{\alpha} b'^{\beta} \rangle, \quad (2.3)$$

and p_M is the fluctuating part of the MHD pressure $p_M (\equiv p + \mathbf{b}^2/2)$.

The production rate P_W (2.2a) expresses the coupling of the turbulent correlations, \mathcal{R} and \mathbf{E}_M , with the mean-field inhomogeneity, $\partial B^a/\partial x^b$ and $\mathbf{\Omega} (= \nabla \times \mathbf{U})$. Exactly the same terms but with the opposite sign appear in the equation of the mean-field cross helicity $\mathbf{U} \cdot \mathbf{B}$ (Yokoi 2010). Hence, the production of the turbulent cross helicity arises from the sink or drain of the mean cross helicity. In this sense, P_W is caused by the cascade of the cross helicity. Other generation mechanisms are related to the transport rate T_W . As can be seen its divergence form, T_W can only contribute to the total amount of turbulent cross helicity through a net flux at the boundary. In the presence of inhomogeneities, parts of T_W may act as local cross-helicity generation mechanisms. The most important effect is inhomogeneity along the magnetic field. If we have energy inhomogeneity along the mean magnetic field, $\mathbf{B} \cdot \nabla K$, cross helicity is produced.

In a compressible MHD case, in addition to these three terms, we have some other generation mechanisms. They will be referred to in section 3.3 in the context of the flow near a sunspot.

3. Numerical simulations

Here we describe three numerical simulations: (i) direct numerical simulation of the local Kolmogorov flow with an imposed magnetic field, (ii) global direct simulation of a rotating spherical fluid shell, and (iii) large-eddy simulation of the local compressible flow near a sunspot.

3.1. DNS of Kolmogorov Flow

The Kolmogorov flow is a three-dimensional periodic flow with a mean velocity shear generated by a sinusoidal external forcing:

$$\mathbf{f} = (f^x, f^y, f^z) = (f_0 \sin 2\pi y/L_y, 0, 0) \quad (3.1)$$

(L_x, L_y, L_z : box dimension). The flow is homogeneous in the x and z directions. Because of this simplicity, the Kolmogorov flow provides a good test for investigating three-dimensional inhomogeneous turbulence with velocity shear and anisotropy (e.g., Sarris *et al.* 2007 and works cited therein. Also see Hamba 1992). In order to see the basic properties of MHD turbulence, in addition to the external forcing, we impose a large-scale magnetic field in the y direction (figure 2). The operator $\langle \dots \rangle$ denotes averaging over the homogeneous (x and z) directions and over an appropriate time. The primed quantities correspond to deviations from the averages.

First we examine the turbulent electromotive force $\mathbf{E}_M = \langle \mathbf{u}' \times \mathbf{b}' \rangle$ in the Kolmogorov flow. We showed the spatial distribution of the z component of $\langle \mathbf{u}' \times \mathbf{b}' \rangle$ in figure 3. It is sinusoidal, as expected from the external forcing. In figure 3, we also showed each term of the r.h.s. in (1.4). The α - or helicity-related term is much less than the β - or turbulent magnetic diffusivity-related term and γ - or cross helicity-related term. Obviously, the main balance in the turbulent electromotive force is attained by the balance between the β - and γ -related terms as

$$\langle \mathbf{u}' \times \mathbf{b}' \rangle \simeq -\beta \mathbf{J} + \gamma \mathbf{\Omega}. \quad (3.2)$$

Next we consider the cross-helicity generation mechanism in the Kolmogorov flow. For

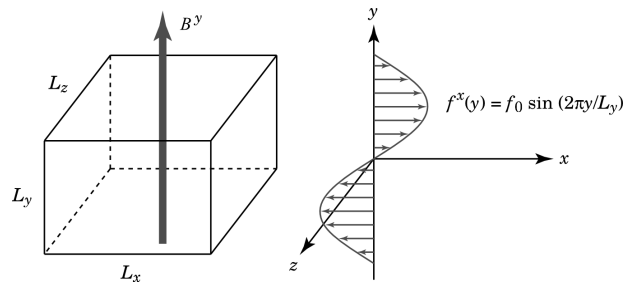


FIGURE 2. Kolmogorov flow with a magnetic field imposed.

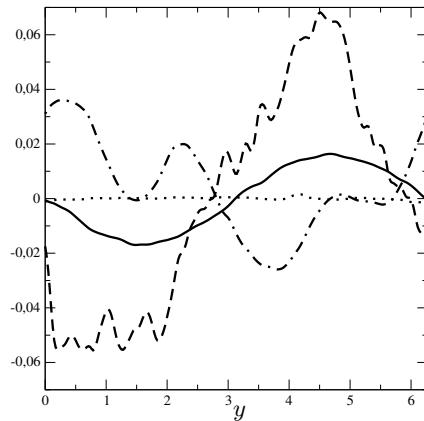


FIGURE 3. Spatial distribution of the turbulent electromotive force and each dynamo term in the Kolmogorov flow versus y : — $\langle \mathbf{u}' \times \mathbf{b}' \rangle^z$; αB^z ; - - - $-\beta J^z$; - · - $\gamma \Omega^z$.

this purpose, we show the spatial distribution of the turbulent cross helicity scaled by the characteristic time of turbulence, W/τ , in figure 4. We also plot the two terms of the turbulent cross-helicity production rate, $-\mathcal{R}^{ab}(\partial b^a/\partial x^b)$ and $-\mathbf{E}_M \cdot \boldsymbol{\Omega}$, and the term related to the energy inhomogeneity along the mean magnetic field, $\mathbf{B} \cdot \nabla K$. This figure shows that the spatial distribution of the turbulent cross helicity is in good agreement with the counterparts of the cross-helicity generation mechanisms. Of course we need to delve further into the detailed budget of cross-helicity evolution including the dissipation and transport rates. Nevertheless, this preliminary result suggests that the production rates can provide a good measure for turbulent cross helicity itself. In actual observations, we often encounter a situation where the direct measurement of the cross helicity is hard or impossible to achieve. In such a situation, if we can measure the production rate of cross helicity, we may estimate the turbulent cross helicity.

We note here without any figure that the magnitude of the turbulent cross helicity scaled by the turbulent MHD energy, $|W|/K = 2|\langle \mathbf{u}' \cdot \mathbf{b}' \rangle|/(\langle \mathbf{u}'^2 + \mathbf{b}'^2 \rangle)$, in this Kolmogorov flow is $O(10^{-2})$. This quantity is very important in magnetic-field generation and in momentum transport. We return to this point later in section 4.

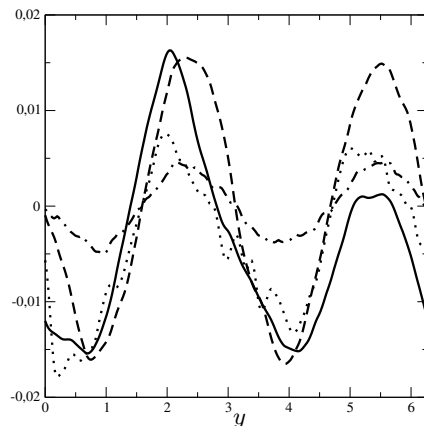


FIGURE 4. Spatial distribution of the turbulent cross helicity and its production-rate terms in the Kolmogorov flow versus y : — W/τ ; ···· $-\mathcal{R}^{ab}(\partial B^a/\partial x^b)$; - - - $-\mathbf{E}_M \cdot \boldsymbol{\Omega}$; - · - $\mathbf{B} \cdot \nabla K$.

3.2. DNS of Spherical Shell

As was mentioned in section 1, a finite cross helicity indicates the breakage of mirror-symmetry in the system. In this sense, the symmetric properties of the cross-helicity distribution in relation to the configuration of the large-scale magnetic field is an interesting point. If the cross helicity is related to the magnetic-field generation mechanism, the configuration of the generated field should reflect the symmetry properties of the spatial distribution of the cross helicity. With the aid of the direct numerical simulations (DNSs) of rotating spherical shells, we investigate this symmetry relation between the magnetic field and cross helicity. In the simulation, gravity-induced convection is caused by a fixed temperature gradient: hot at the inner boundary and cold at the outer boundary. The Boussinesq approximation is assumed, where the density ρ variation is taken into account only through the gravity term. For further details of these simulations, see Simitev & Busse (2005) and works cited therein.

The properties of the flow and magnetic field change depending on simulation parameters such as the Rayleigh, Coriolis, Prandtl, and magnetic Prandtl numbers. In some cases the generated magnetic-field configuration is dipole-like, and in other cases it is quadrupole-like. First, we show the spatial distributions of the cross and kinetic helicities in the dipole- and quadrupole-like large-scale magnetic-field configurations in figure 5. The plots in the top row show the dipole-like configuration case. The plots on the left show the lines of constant toroidal magnetic field (in the left half) and poloidal magnetic field (in the right half). These magnetic fields exhibit a dipole-like configuration: anti-symmetric with respect to the equatorial plane. In correspondence to this magnetic-field configuration, the plots on the right show the lines of constant cross helicity (in the left half) and kinetic helicity (in the right half). The cross helicity exhibits an anti-symmetric distribution with respect to the equatorial plane, while the kinetic helicity has a symmetric distribution. The plots in the bottom row show the quadrupole-like configuration case. The plots on the left show quadrupole-like configurations of the toroidal and poloidal magnetic fields: symmetric with respect to the equatorial plane. In this case, the plots on the right show contours of the cross helicity (in the left half) and

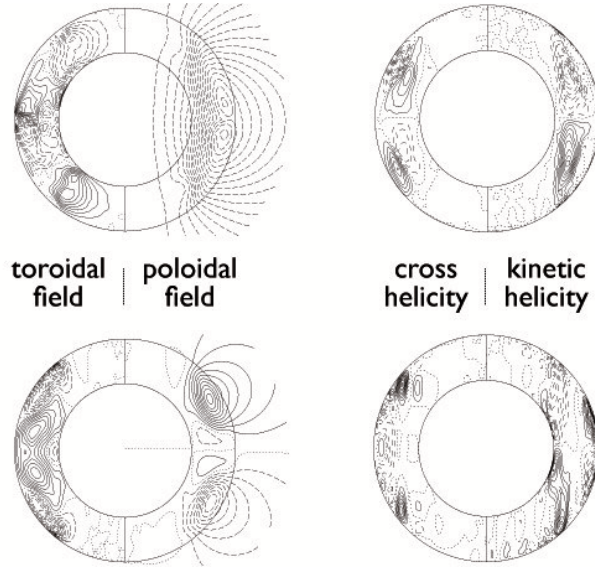


FIGURE 5. Spatial distribution of the turbulent cross and kinetic helicities in the dipole- and quadrupole-like magnetic configurations in spherical shell flows.

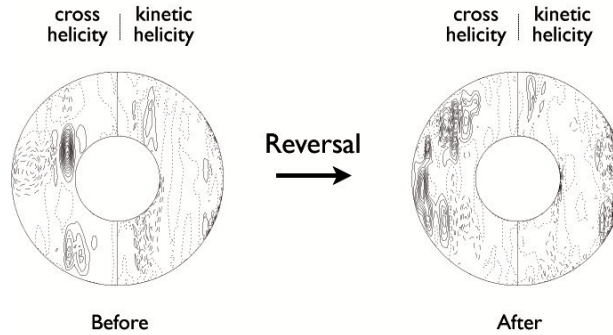


FIGURE 6. Spatial distribution of the cross and kinetic helicities during the magnetic-field reversal.

kinetic helicity (in the right half). The cross helicity exhibits a symmetric distribution with respect to the equatorial plane, while the kinetic helicity has an anti-symmetric one.

It is well known that the large-scale magnetic-field configurations of the Sun and the Earth change with time, although the regularities of the change differ significantly in these two cases. In both cases, it is quite important to understand what causes the reversal of the magnetic field. With this point in mind, we examine the signs of pseudo-scalars during magnetic-field reversal. In figure 6, the plot on the left shows contours of the cross helicity (in the left half) and the kinetic helicity (in the right half) before the field reversal in the dipole-like field configuration case. After the reversal, the contours change to the plot in the right.

We see from these plots that the cross helicity changes its sign during the field reversal whereas the kinetic helicity does not. This result suggests that it is not the temporal behavior of the kinetic helicity but of the cross helicity that affects the temporal behavior

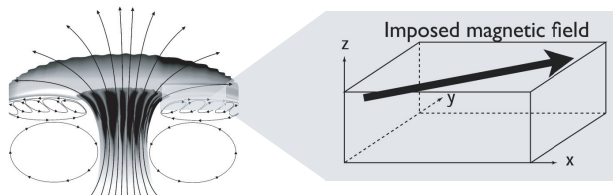


FIGURE 7. A box mimicking a local flow region near the sunspot.

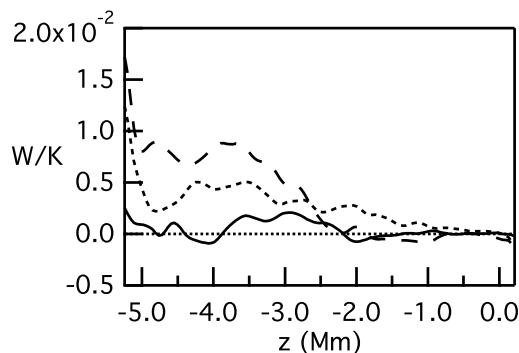


FIGURE 8. Spatial distribution of the turbulent cross helicity scaled by the turbulent MHD energy as a function of the depth in the solar convection zone: — $B = 600$ G; 1200 G; ---- 1500 G.

of the large-scale magnetic field. In some sense, this result is natural since the cross helicity changes its sign under the transformation of the magnetic-field reversal: $\mathbf{b} \rightarrow -\mathbf{b}$, while neither the kinetic helicity nor current helicity does. In order to determine the causal relation, we should scrutinize the evolution of cross helicity and magnetic fields.

3.3. LES of Sunspot Flow

Despite recent developments in helioseismology, it is still not easy to simultaneously observe the velocity and magnetic field inside the Sun. Thus, simulations of the solar convection zone with realistic parameters are important to understand the physical processes of generating the magnetic field and sustaining the differential rotation of the Sun. With the aid of large-eddy simulation (LES), using appropriate sub-grid scale (SGS) models, we address such phenomena inside the Sun, in order to provide a basis for analyzing and interpreting the observational data.

We consider a slab mimicking a local region of the flow around a sunspot (figure 7). A large-scale magnetic field inclined by 85° toward the surface (almost horizontal) is imposed. We perform numerical simulations with different magnetic-field strengths (600, 1000, and 1200 G). The results of this type of numerical simulation reveal several physical processes inside the Sun including self-organization in the solar convection zone. For details of numerical simulations, see e.g., Jacoutot *et al.*, (2008); Kitiashvili *et al.* (2009). In this work, we focus our attention on the cross-helicity effect.

In figure 8, we plot the turbulent cross helicity scaled by the turbulent MHD energy against the depth from the surface. Our calculations indicate that the turbulent cross helicity itself is distributed in both the shallow and deep regions. However, velocity and

magnetic fluctuations (turbulent MHD energy per unit mass) are distributed more in the shallow region than in the deep region. As a result, the scaled cross helicity is much larger in the deep region, where the magnitude of W/K is $O(10^{-2})$.

Analysis of the cross-helicity generation mechanisms in this simulation of the solar convection zone is in progress. There are some cross-helicity generation mechanisms other than P_W (2.2a) and $\mathbf{B} \cdot \nabla K$ [in (2.2c)]. They are related to the mean-density stratification, inhomogeneities of a kind of heat flux such as

$$\frac{W}{2\bar{\rho}} \mathbf{U} \cdot \nabla \bar{\rho}, \quad -\nabla \cdot \langle p' \mathbf{b}' \rangle \quad (3.3)$$

(Yokoi & Hamba 2007; Yokoi *et al.* 2008). Among (2.2a), (3.3) and the first term of (2.2c), according to the preliminary analysis, heat-flux inhomogeneity seems to be dominant, although further analysis is warranted.

4. Discussion

The DNS of the Kolmogorov flow (section 3.1) showed the importance of the cross-helicity effect in the turbulent electromotive force in comparison to the α or helicity effect in an inhomogeneous shear flow. On the other hand, the DNS of the spherical shell of fluid (section 3.2) showed that the symmetry of the large-scale magnetic field reflects the sign of cross helicity rather than that of kinetic helicity. These results indicate the relative importance of the cross-helicity effect in the dynamo processes. Thus it is important to know how much cross helicity is present in turbulence.

From the practical viewpoint of applications to astro/geophysical phenomena, the most important quantity is not the value of cross helicity itself but of the scaled one:

$$\frac{W}{K} = \frac{\langle \mathbf{u}' \cdot \mathbf{b}' \rangle}{\langle \mathbf{u}'^2 + \mathbf{b}'^2 \rangle / 2}. \quad (4.1)$$

Yoshizawa & Yokoi (1993) showed $\mathbf{B} \propto (W/K)\mathbf{U}$ is a special solution of the stationary cross-helicity dynamo. From satellite observations of solar-wind turbulence, it is known that W/K is almost one near the Sun (Tu & Marsch 1995). When compared with such a high correlation, the value of $O(10^{-2})$ we obtained in the numerical simulations may look very small. However, this is not the case. For instance, in applying the cross-helicity dynamo to the global magnetic-field structure in spiral galaxies, $|W|/K = O(10^{-2})$ was shown to be enough to elucidate the strength of the galactic magnetic field (Yokoi 1996). To estimate the magnitude of torsional oscillation in the solar convection zone, the value of W/K is considered to be important. If the magnitude of cross helicity is $|W|/K = O(10^{-2})$, the cross-helicity effect must play a key role in the torsional oscillation mechanism. However, if the value is something like $O(10^{-5})$, the magnitude of torsional oscillation cannot be considered as a result of the cross-helicity effect.

In the preliminary LES calculation of the flow near a sunspot (section 3.3), the scaled cross helicity is estimated as $|W|/K = O(10^{-2})$ in the deeper region of the calculation domain. This result suggests that the cross-helicity effect is large enough and should be incorporated into the theoretical formulation and turbulence modeling of the solar convection zone.

5. Concluding remarks

Cross-helicity effects were investigated from several different approaches including theories, observations, and numerical simulations. Here we focused on the numerical aspect of this diverse work. The DNSs of the Kolmogorov flow and the spherical shell fluid validated the cross-helicity effect in comparison to the well-known α effect. We calculated how much cross helicity is present in turbulence, and examined several possible generation mechanisms. In addition to production arising from the cross-helicity cascade, we determined that one should take account of other mechanisms, such as inhomogeneities along the large-scale magnetic field. Theoretical and numerical results, such as the anti-symmetric distribution of cross helicity, should be validated by solar observations. Relationships such as the one between the cross-helicity distribution and the generation mechanisms may be utilized for estimating observationally unavailable quantities.

REFERENCES

- HAMBA, F., 1992 Turbulent dynamo effect and cross helicity in magnetohydrodynamic flows. *Phys. Fluids A* **4**, 441-450.
- JACOUTOT, L., KOSOVICHEV, A. G., WRAY, A. & MANSOUR, N. N., 2010 Realistic numerical simulations of solar convection and oscillations in magnetic regions. *Astrophys. J.* **684**, L51-L54.
- KITIASHVILI, I. N., KOSOVICHEV, A. G., WRAY, A. A. & MANSOUR, N. N. 2009 Traveling waves of magnetoconvection and the origin of the Evershed effect in sunspot. *Astrophys. J.* **700**, L178-L181.
- KRAUSE, F. & RÄDLER, K.-H. 1980 *Mean-Field Magnetohydrodynamics and Dynamo Theory*. Pergamon Press.
- POUQUET, A., FRISCH, U. & LÉORAT, J. 1976 Strong MHD helical turbulence and the nonlinear dynamo effect. *J. Fluid Mech.* **77**, 321-354.
- SARRIS, I. E., JEANMART, H., CARATI, D. & WINCKELMANS, G. 2007 Box-size dependence and breaking of translational invariance in the velocity statistics computed from three-dimensional turbulent Kolmogorov flows. *Phys. Fluids* **19**, 095101-1-9.
- SIMITEV, R. & BUSSE, F. H. 2005 Prandtl-number dependence of convection-driven dynamos in rotating spherical fluid shells. *J. Fluid Mech.* **532**, 365-388.
- TU, C.-Y. & MARSCH, E. 1995 *MHD Structures, Waves and Turbulence in the Solar Wind*. Kluwer Academic Publisher.
- YOKOI, N. 1996 Large-scale magnetic fields in spiral galaxies viewed from the cross-helicity dynamo. *Astron. Astrophys.* **311**, 731-745.
- YOKOI, N. 1999 Magnetic-field generation and turbulence suppression due to cross-helicity effects. *Phys. Fluids* **11**, 2307-2316.
- YOKOI, N. 2010 Modeling the turbulent cross-helicity evolution: Production, dissipation, and transport rates. *J. Turbulence* (submitted).
- YOKOI, N. & HAMBA, F. 2007 An application of the turbulent magnetohydrodynamic residual-energy equation model to the solar wind. *Phys. Plasmas* **14**, 112904-1-16.
- YOKOI, N., RUBINSTEIN, R., YOSHIKAWA, A. & HAMBA, F. 2008 A turbulence model for magnetohydrodynamic plasmas. *J. Turbulence* **9**, N37-1-25.
- YOSHIKAWA, A. 1990 Self-consistent turbulent dynamo modeling of reversed field pinches and planetary magnetic fields. *Phys. Fluids B* **2**, 1589-1600.
- YOSHIKAWA, A. & YOKOI, N. 1993 Turbulent magnetohydrodynamic dynamo for accretion disks using the cross-helicity effect. *Astrophys. J.* **407**, 540-548.